


Article

Nonlinear Robust Fault-Tolerant Tracking Control of a Tri-Rotor UAV Against Actuator's Abnormal Behavior

Wenlai Ma ^{1,2}, Minghua Hu ¹, Wei Hao ^{2,*} , Haijun Wang ² and Peiyu Wang ²¹ College of Civil Aviation, Nanjing University of Aeronautics and Astronautics, Nanjing 210016, China² Flight College, Binzhou University, Binzhou 256600, China

* Correspondence: haowei0923@tju.edu.cn

Abstract: In this paper, a new nonlinear robust fault-tolerant tracking control method is proposed for a tri-rotor unmanned aerial vehicle (UAV) under unknown abnormal actuator behaviors together with unknown external disturbances. The actuator anomalies are modeled as time-varying multiplicative parameters to improve the model accuracy. The control system is decoupled into two parts, including the inner-loop attitude control and the outer-loop position control. The radial basis function neural network (RBFNN) is utilized in the outer loop to estimate the actuator anomalies and external disturbances, and then the state feedback controller is employed for the position tracking of the UAV. Then, the robust integral of the signum of the error (RISE) controller is designed for the inner loop to compensate for actuator anomalies and external disturbances. The composite stability of the closed-loop system and the asymptotical tracking performance are proved via a Lyapunov-based stability analysis. Numerical simulations based on the proposed fault tolerant control (FTC) scheme as well as the comparison results with a sliding mode-based FTC method validate the effectiveness and better performance of the proposed control design.

Keywords: tri-rotor UAV; FTC; robust tracking control; inner-outer-loop control



Citation: Ma, W.; Hu, M.; Hao, W.; Wang, H.; Wang, P. Nonlinear Robust Fault-Tolerant Tracking Control of a Tri-Rotor UAV Against Actuator's Abnormal Behavior. *Actuators* **2023**, *12*, 140. <https://doi.org/10.3390/act12040140>

Academic Editor: Anyang Lu

Received: 10 February 2023

Revised: 22 March 2023

Accepted: 24 March 2023

Published: 26 March 2023



Copyright: © 2023 by the authors. Licensee MDPI, Basel, Switzerland. This article is an open access article distributed under the terms and conditions of the Creative Commons Attribution (CC BY) license (<https://creativecommons.org/licenses/by/4.0/>).

1. Introduction

In recent years, the multi-rotor unmanned aerial vehicle (UAV) has attracted increasing attention for both military and civil applications, such as fire surveillance, agricultural survey, and so on [1,2]. Different from other multi-rotor UAVs, the tri-rotor UAV shows some unique advantages, such as a simpler structure, lower cost, lower energy consumption, and higher maneuverability [3,4]. The mechanical structure of a tri-rotor UAV consists of two fixed motors and one tilt motor equipped on a rear servo [5]. Therefore, the movement of the tri-rotor UAV is generated by the rotation of the three motors and deflection of the tilt rear servo, which are the so-called actuators [6]. Meanwhile, with the development of the tri-rotor UAV, the frequent occurrence of abnormal behaviors of the UAV has been inevitable [7]. In fact, with the continuous operation of the actuators, the risk of anomalies from the actuators anomalies is greatly increased; thus, the tri-rotor UAV could become unstable or even out of control, which makes the fault-tolerant control (FTC) of the tri-rotor UAV significant [8]. As we all know, the tri-rotor UAV has six DOFs with only four inputs, which is a typical underactuated system and which therefore makes the situation more serious when anomalies of the actuators happen [9]. Most existing works are mainly focused on the dynamic modeling and flight control of tri-rotor UAVs. In [10], a dynamic model of a tri-rotor UAV was obtained via the Newton–Euler approach, and then the saturating-function-based sequential control strategy was utilized to realize the position tracking control, which was verified through real-time experiments on a self-built Simulink-based platform. In [11], a PID-based attitude control and a linear quadratic translational control for a tri-rotor UAV was presented, and numerical simulation results demonstrated its efficiency. In [12], an adaptive hybrid scheme was utilized for the attitude

and altitude control of a tri-rotor UAV. The numerical simulation results showed a better transient response with a low overshoot and undershoot to achieve the desired attitude. What can be concluded from the above is that studies on tri-rotor UAVs mainly focus on dynamic modeling and flight control, which have been validated by numerical simulations or real-time experiments, while quite few studies have taken the FTC of tri-rotor UAVs into consideration.

Apart from tri-rotor UAVs, studies of the FTC of other types of multi-rotor UAVs, such as quadrotor UAVs and hexacopter UAVs, may also bring us inspiration. For the FTC of quadrotor UAVs and hex-rotor UAVs, algorithms such as PID control [13], adaptive control [14], sliding mode control [15], and robust control [16] have been utilized [17,18]. In [19], a data-driven fault-tolerant synchronization control scheme based on a distributed observer and optimal control policy was investigated for unknown cooperative quadrotors subject to nonlinearities and multiple actuator anomalies in the quadrotor dynamics. In [20], two FTC designs based on gain-scheduling H_∞ control were presented for a multi-copter UAV subject to actuator anomalies. In [21], the authors surveyed the trajectory tracking issue of underactuated vertical takeoff and landing UAVs subject to a loss of efficiency and actuator biases. In [22], an active FTC strategy was proposed for time-varying actuator anomalies, and the time-delay phenomenon caused by fault diagnosis was discussed. In [23], an adaptive FTC allocation method was presented to solve the trajectory tracking problem of a hexacopter UAV against degradation and failures of the propulsion system without accurate fault information and online optimization. The effectiveness of the proposed FTC strategies were verified through real-time flight experiments, and the control performances were analyzed quantitatively.

In our previous work [24,25], nonlinear FTC laws were designed to maintain the stability of a tri-rotor UAV under an unknown rear servo's stuck fault, and real-time experiments validated the robust performance. To further address our research, an inner-outer-loop-based fault-tolerant tracking control strategy is developed for the tri-rotor UAV, and the main contributions of this article can be summarized as follows. First, the actuator anomalies of the tri-rotor UAV are taken into consideration, while most existing works do not consider this issue, which is modeled as some time-varying multiplicative parameters to improve the model accuracy. Second, the control system is decoupled into the inner-loop attitude control and outer-loop position control. For the outer loop, approximation components based on RBFNN are introduced to estimate the unknown external disturbances and actuator anomalies, and then the state feedback algorithm is employed to design the position controller [26,27]. For the inner loop, a RISE-based controller is developed to compensate for the unknown exogenous disturbances together with actuator anomalies without an additional fault isolation and reconstruction mechanism [28]. Third, the composite stability of the cascaded system is proved by Lyapunov theory. Finally, numerical simulations and the comparison with sliding mode (SM) methodology are provided to illustrate the better tracking performance of the proposed FTC strategy. To our best knowledge, few existing works have taken the FTC of tri-rotor UAV into consideration, and the control methods proposed in this article also have not been utilized in the control of a tri-rotor UAV.

This paper is organized as follows. The dynamics of the tri-rotor UAV under actuator anomalies are described in Section 1. In Sections 2 and 3, the design of the FTC scheme and the composite stability analysis are presented. Numerical simulation results are shown in Section 4. Finally, some conclusion remarks are included in Section 5.

2. Problem Formulation

In order to describe the dynamics and kinematics of a tri-rotor UAV, two right-hand coordinate systems are utilized. One is the inertial frame represented by $\{\mathcal{I}\} = \{x_{\mathcal{I}}, y_{\mathcal{I}}, z_{\mathcal{I}}\}$, the origin of which is attached on the ground, with $z_{\mathcal{I}}$ being the vertical direction downward into the ground, $y_{\mathcal{I}}$ being the east direction, and $x_{\mathcal{I}}$ being determined by the right-hand rule. The other one is the body-fixed frame represented by $\{\mathcal{B}\} = \{x_{\mathcal{B}}, y_{\mathcal{B}}, z_{\mathcal{B}}\}$, which is

centered at the centroid of the tri-rotor UAV. The body axis z_B is the normal axis of the principal plane of the tri-rotor UAV directed from top to bottom, the body axis x_B is along with the backward flying direction of the tri-rotor, and the direction of the body axis y_B is determined by the right-hand rule, as illustrated in Figure 1.

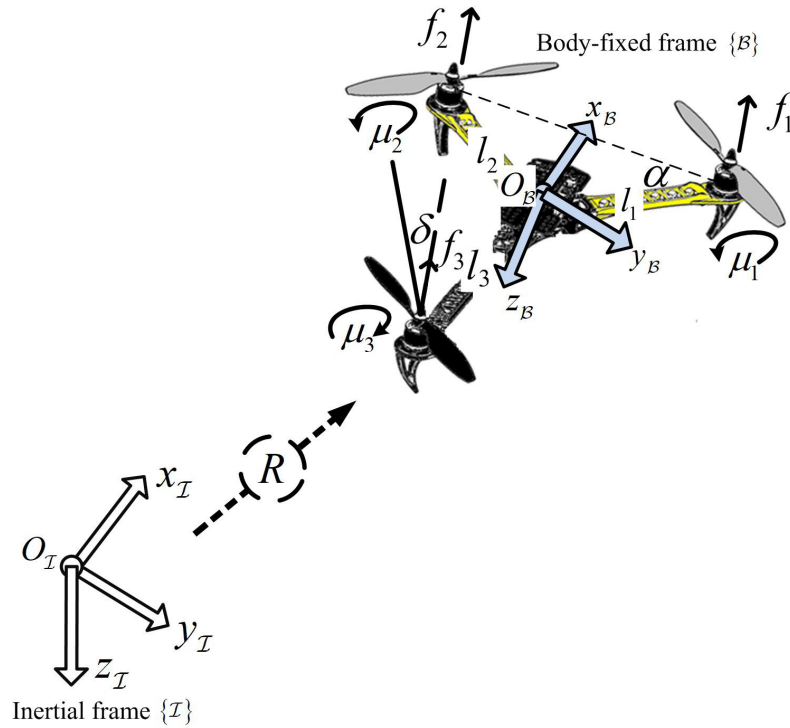


Figure 1. Schematic of tri-rotor UAV.

In Figure 1, motor 1 and motor 2 rotate clockwise, and motor 3 rotates anti-clockwise. Meanwhile, the relationship between the rotational torques and the thrust force generated by the three motors can be illustrated via the following equation,

$$\begin{cases} \tau_\phi = f_1 l_1 \cos \alpha - f_2 l_2 \cos \alpha \\ \tau_\theta = -(f_1 l_1 + f_2 l_2) \sin \alpha + f_3 \cos \delta \cdot l_3 - \mu_3 \sin \delta \\ \tau_\psi = -\mu_1 - \mu_2 + \mu_3 \cos \delta + f_3 \sin \delta \cdot l_3 \\ F = -f_1 - f_2 - f_3 \cos \delta \end{cases}, \quad (1)$$

where the symbols $F(t)$ and $\tau(t) = [\tau_\phi(t) \quad \tau_\theta(t) \quad \tau_\psi(t)]^T \in \mathbb{R}^3$ denote the total thrust force and rotational torques produced by the three motors and the rear servo, and the symbols f_i and μ_i , ($i = 1, 2, 3$) represent the thrust and anti-torque produced by the i th motor, respectively. The constant l_i , ($i = 1, 2, 3$) denotes the distance between the i th motor and the origin O_B . Supposing there was a line connecting motor 1 to motor 2 and another connecting motor 1 to the origin O_B , then an angle would be formulated between these two lines, which is denoted by α . The signal δ represents the angle by which the rear servo deviates from the plane of $X_B O_B Z_B$, with clockwise being the positive direction.

For the convenience of the subsequent control development, the following assumptions are proposed.

Assumption 1. The structure of the tri-rotor UAV is symmetrical with respect to the axis of $O_B X_B$, so the equation of $l_1 = l_2 = l$ is established, where l is a constant.

Assumption 2. The terms of $f_3 \sin \delta$ are neglected, and $\cos \delta$ equals to 1 since the angle $\delta(t)$ varies within a quite small range. Actually, the normal variation range of the angle $\delta(t)$ is bounded within 0.056 rad.

When Assumptions 1 and 2 are all satisfied(1) and can be rewritten as follows:

$$\begin{cases} \tau_\phi = (f_1 - f_2)l \cos \alpha \\ \tau_\theta = -(f_1 + f_2)l \sin \alpha + f_3 \cos \delta \cdot l_3 \\ \tau_\psi = -\mu_1 - \mu_2 + \mu_3 \cos \delta \\ F = -f_1 - f_2 - f_3 \cos \delta \end{cases} \quad (2)$$

The Euclidean position and Euler angle of the UAV with respect to the frame $\{\mathcal{I}\}$ are represented by $\zeta(t) = [x(t) \ y(t) \ z(t)]^T \in \mathbb{R}^3$ and $\eta(t) = [\phi(t) \ \theta(t) \ \psi]^T \in \mathbb{R}^3$, and then the dynamic model of the tri-rotor UAV expressed in $\{\mathcal{I}\}$ is given in the following form [29]:

$$\begin{cases} m\ddot{\zeta} = -FR(\eta)e_3 + mge_3 + d_\zeta \\ M(\eta)\ddot{\eta} = -C(\eta, \dot{\eta})\dot{\eta} + \Psi^T(\eta)\tau + \Psi^T(\eta)d_\eta \end{cases} \quad (3)$$

where $m \in \mathbb{R}^+$ denotes the mass of the UAV, $M(\eta)$ is a positive definite inertial matrix, $C(\eta, \dot{\eta})$ is the Coriolis and centrifugal matrix, g is the acceleration of the gravity, and $e_3 = [0 \ 0 \ 1]^T \in \mathbb{R}^3$, $R(\cdot)$ and $\Psi(\cdot)$ are the rotation matrixes expressed as follows,

$$R(\eta) = \begin{bmatrix} c\theta c\psi & s\phi s\theta c\psi - c\phi s\psi & c\phi s\theta c\psi + s\phi s\psi \\ c\theta s\psi & s\phi s\theta s\psi + c\phi c\psi & c\phi s\theta s\psi - s\phi c\psi \\ -s\theta & s\phi c\theta & c\phi c\theta \end{bmatrix}, \quad (4)$$

$$\Psi(\eta) = \begin{bmatrix} 1 & 0 & -s\theta \\ 0 & c\phi & c\theta s\phi \\ 0 & -s\phi & s\theta c\phi \end{bmatrix}, \quad (5)$$

where s and c are abbreviations for $\sin(\cdot)$ and $\cos(\cdot)$. In (3), $d_\zeta(t) = [d_x(t) \ d_y(t) \ d_z(t)]^T \in \mathbb{R}^3$ and $d_\eta(t) = [d_\phi(t) \ d_\theta(t) \ d_\psi(t)]^T \in \mathbb{R}^3$ represent the unknown external disturbances.

Because of the singularity of the tri-rotor UAV system at $\theta(t) = \pm\pi/2$, the following assumption is presented.

Assumption 3. The UAV's pitch angle $\theta(t)$ satisfies $\theta(t) \neq \pm\pi/2$.

For the convenience of the subsequent control development, the dynamic model of the tri-rotor UAV in (3) can be rewritten as

When the actuator anomalies occur in the tri-rotor UAV, the total thrust force $F(t)$ and rotational torque $\tau(t)$ will be decreased to some extent. Then, the fault dynamics of the tri-rotor UAV can be obtained as follows.

$$\begin{cases} \ddot{\zeta} = -\frac{1}{m}FR(\eta)e_3 + ge_3 + \underbrace{\frac{1}{m}d_\zeta + \Lambda_\zeta F}_{D_\zeta(t)} \\ \ddot{\eta} = \underbrace{-M^{-1}C\dot{\eta} + \psi^{-1}J^{-1}\tau}_{\tilde{\tau}} + \underbrace{\psi^{-1}J^{-1}d_\eta + \Lambda_\eta \tau}_{D_\eta(t)} \end{cases} \quad (6)$$

where $\Lambda_\zeta(t) = [\lambda_x(t) \ \lambda_y(t) \ \lambda_z(t)]^T \in \mathbb{R}^3$, $\Lambda_\eta(t) = [\lambda_\phi(t) \ \lambda_\theta(t) \ \lambda_\psi(t)]^T \in \mathbb{R}^3$, $\lambda_i(t) \in [0, 1]$, $i \in \{x, y, z, \phi, \theta, \psi\}$ and different values of the parameter λ_i means different actuator anomalies, which are listed as follows:

$$\begin{cases} \lambda_i(t) = 0, & \text{no anomaly happens} \\ 0 < \lambda_i(t) < 1, & \text{partial anomaly} \\ \lambda_i(t) = 1, & \text{total anomaly} \end{cases} \quad (7)$$

In (6), $\tilde{\tau}(t)$, $D_\zeta(t)$, $D_\eta(t)$ are some variable substitutions, which are defined as follows.

$$\tilde{\tau} = -M^{-1}C\dot{\eta} + \psi^{-1}J^{-1}\tau, \tag{8}$$

$$D_{\tilde{\zeta}}(t) = \frac{1}{m}d_{\tilde{\zeta}} + \Lambda_{\tilde{\zeta}}F, \tag{9}$$

$$D_{\eta}(t) = \psi^{-1}J^{-1}d_{\eta} + \Lambda_{\eta}\tau, \tag{10}$$

Assumption 4. From the above, we know that $\|d_{\tilde{\zeta}}\| \leq \bar{d}_{\tilde{\zeta}}, \|\Lambda_{\tilde{\zeta}}\| \leq 1$, the total thrust $F(t)$ and rotational torques $\tau(t)$ are bounded, i.e. $\|\Lambda_{\tilde{\zeta}}F\| \leq \bar{\Lambda}_{\tilde{\zeta}}F, \|\Lambda_{\eta}\tau\| \leq \bar{\Lambda}_{\eta}\tau$, and therefore, $\|D_{\tilde{\zeta}}\| \leq \bar{D}_{\tilde{\zeta}}, \|D_{\eta}\| \leq \bar{D}_{\eta}$, where $\bar{\Lambda}_{\tilde{\zeta}}F, \bar{\Lambda}_{\eta}\tau, \bar{D}_{\tilde{\zeta}}, \bar{D}_{\eta}$ are some unknown bounded constants.

Remark 1. The overall control object is to design the total thrust $F(t)$ and rotational torques $\tau(t)$ to ensure the tri-rotor UAV track's time-varying trajectories under actuator anomalies.

3. Control Development

Let $\tilde{\zeta}_d(t) = [x_d(t) \ y_d(t) \ z_d(t)]^T \in \mathbb{R}^3$ be the desired position, and then the position tracking error $e_{\tilde{\zeta}}(t) = [e_x(t) \ e_y(t) \ e_z(t)]^T \in \mathbb{R}^3$ and the filtered error $s_{\tilde{\zeta}}(t) = [s_x(t) \ s_y(t) \ s_z(t)]^T \in \mathbb{R}^3$ are obtained as

$$e_{\tilde{\zeta}} = \tilde{\zeta} - \tilde{\zeta}_d, \tag{11}$$

$$s_{\tilde{\zeta}} = \dot{e}_{\tilde{\zeta}} + \alpha_{\tilde{\zeta}}e_{\tilde{\zeta}}. \tag{12}$$

After taking the time derivative of (12) and substituting (6) together with (11) into the resulting equation, the position error dynamics can be obtained as

$$\dot{s}_{\tilde{\zeta}} = -\frac{1}{m}FR(\eta)e_3 + ge_3 + D_{\tilde{\zeta}} + \alpha_{\tilde{\zeta}}\dot{e}_{\tilde{\zeta}} - \ddot{\zeta}_d. \tag{13}$$

The dynamics described in (6) can be considered a cascaded structure where the position and attitude subsystem are coupled through the rotation matrix $R(\eta)$. Hence, to formulate the problem as the control of two connected systems, a virtual control vector $v = [v_x \ v_y \ v_z]^T \in \mathbb{R}^3$ defined as $v = -\frac{1}{m}FR(\eta_d)e_3 + ge_3$ is introduced.

$$\begin{cases} v_x = \frac{F}{m}(c\phi_d s\theta_d c\psi_d + s\phi_d s\psi_d) \\ v_y = \frac{F}{m}(c\phi_d s\theta_d s\psi_d - s\phi_d c\psi_d) \\ v_z = \frac{F}{m}(c\phi_d c\theta_d) - g \end{cases}, \tag{14}$$

$$\Rightarrow \begin{cases} F = m\sqrt{v_x^2 + v_y^2 + (v_z + g)^2} \\ \phi_d = \arcsin\left(\frac{m}{F}(v_x s\psi_d - v_y c\psi_d)\right) \\ \theta_d = \arctan\left(\frac{v_x c\psi_d + v_y s\psi_d}{v_z + g}\right) \end{cases}. \tag{15}$$

Then, the open-loop system can be obtained after introducing v and substituting (6) into (13),

$$\begin{aligned} \dot{s}_{\tilde{\zeta}} &= \underbrace{\alpha_{\tilde{\zeta}}\dot{e}_{\tilde{\zeta}} - \ddot{\zeta}_d + v + D_{\tilde{\zeta}}}_{f_{\tilde{\zeta}}(\dot{e}_{\tilde{\zeta}}, v, \ddot{\zeta}_d)} + \underbrace{\frac{1}{m}Fh(\eta_d, e_{\eta})}_{\Delta(F, \eta_d, e_{\eta})} \\ &= f_{\tilde{\zeta}}(\dot{e}_{\tilde{\zeta}}, v, \ddot{\zeta}_d) + \Delta(F, \eta_d, e_{\eta}), \end{aligned} \tag{16}$$

where $\eta_d(t) = [\phi_d(t) \ \theta_d(t) \ \psi_d(t)]^T \in \mathbb{R}^3$ is the desired attitude and $h(\eta_d, e_{\eta}) = [h_x \ h_y \ h_z]^T$ is obtained as

$$\begin{cases} h_x = c\phi_d s\theta_d c\psi + s\phi_d s\psi - (c\phi_d s\theta_d c\psi_d + s\phi_d s\psi_d) \\ h_y = c\phi_d s\theta_d s\psi - s\phi_d c\psi - (c\phi_d s\theta_d s\psi_d - s\phi_d c\psi_d) \\ h_z = c\phi_d c\theta - c\phi_d c\theta_d \end{cases}. \tag{17}$$

Similar to the above analysis, the attitude tracking error $e_{\eta}(t) = [e_{\phi}(t) \ e_{\theta}(t) \ e_{\psi}(t)]^T \in \mathbb{R}^3$ and the filtered error $s_{\eta}(t) = [s_{\phi}(t) \ s_{\theta}(t) \ s_{\psi}(t)]^T \in \mathbb{R}^3$ are obtained as

$$e_\eta = \eta - \eta_d, \quad (18)$$

$$s_\eta = \dot{e}_\eta + \alpha_\eta e_\eta. \quad (19)$$

After taking the time derivative of (19) and substituting (6) together with (18) into the resulting equation, the attitude error dynamics can be obtained as

$$\dot{s}_\eta = \underbrace{\alpha_\eta \dot{e}_\eta - \ddot{\eta}_d + \tilde{\tau} + D_\eta}_{f_\eta(\dot{e}_\eta, \tilde{\tau}, \ddot{\eta}_d)}. \quad (20)$$

For the system in cascade, one of the most important theorems on its stability analysis is the following theorem expressed in [30].

Theorem 1. *If there is a feedback $v(s_\xi, \ddot{\xi}_d)$ such that $s_\xi = 0$ is an asymptotically stable equilibrium of $\dot{s}_\xi = f_\xi(\dot{e}_\xi, v, \ddot{\xi}_d)$, then any partial state feedback control $\tilde{\tau}(s_\eta, \ddot{\eta}_d)$, which renders the s_η -subsystem equilibrium $s_\eta = 0$ asymptotically stable, also achieves the asymptotic stability of $(s_\xi, s_\eta) = (0, 0)$.*

From Theorem 1 and also according to references [29,31], the main control development can be achieved in the following three steps.

1. Choose the control law $v(s_\xi, \ddot{\xi}_d)$ for the system of $\dot{s}_\xi = f_\xi(\dot{e}_\xi, v, \ddot{\xi}_d)$ without the interconnection term $\Delta(F, \eta_d, e_\eta)$ to ensure the tracking error e_ξ converges to 0 asymptotically.
2. Choose the control law $\tilde{\tau}(s_\eta, \ddot{\eta}_d)$ for the system of $\dot{s}_\eta = f_\eta(\dot{e}_\eta, \tilde{\tau}, \ddot{\eta}_d)$ to ensure the tracking error e_η converges to 0 asymptotically.
3. Prove that s_ξ and s_η converge to 0 asymptotically considering the coupling term $\Delta(F, \eta_d, e_\eta)$.

3.1. Outer-Loop Position Controller Design Based on RBFNN State Feedback Method

For the outer-loop system $\dot{s}_\xi = f_\xi(\dot{e}_\xi, v, \ddot{\xi}_d)$, the objective is to design the auxiliary control input $v(t)$ to ensure that the tracking error e_ξ converges to zero asymptotically.

For the unknown continuous term of D_ξ , we utilize RBFNN to approximate them over the compact set Ω . Then, D_ξ can be re-expressed in the following form:

$$D_\xi = W^{*T} S(e_\xi^T, s_\xi^T) + \varepsilon(e_\xi^T, s_\xi^T), \quad (21)$$

where $W^* \in \mathbb{R}^{q \times 3}$ is the ideal weight with the neuron number q , $S(x) =$

$\begin{bmatrix} s_1(x) & s_2(x) & \cdots & s_q(x) \end{bmatrix}^T$ is the basis function vectors with $s_i(x) = e^{-\frac{(x-\mu_i)^T(x-\mu_i)}{2}}$, $\mu_i = \begin{bmatrix} \mu_{i1} & \mu_{i2} & \cdots & \mu_{i6} \end{bmatrix}^T$ is the center of receptive field, $i = 1, 2, \dots, q$, and $\varepsilon(\cdot)$ is the approximation error. Since the ideal weight matrix W^* is an unknown constant matrix, which is unavailable for the actual control design, we introduce the estimation of the ideal RBFNN weight W^* represented by \hat{W} , which satisfies

$$\dot{\hat{W}} = \Gamma_\xi (S(e_\xi^T, s_\xi^T) s_\xi^T - \sigma_\xi \hat{W}), \quad (22)$$

and the control input $v(t)$ can be expressed as

$$v = -k_\xi s_\xi - \alpha_\xi \dot{e}_\xi + \ddot{\xi}_d - \hat{W}^T S(e_\xi^T, s_\xi^T), \quad (23)$$

where $k_\xi \in \mathbb{R}^{3 \times 3}$ is a positive constant matrix.

By substituting (23) into (16), the closed-loop dynamics of s_ξ can be formulated as

$$\dot{s}_\xi = -k_\xi s_\xi - \tilde{W}^T S(e_\xi^T, s_\xi^T) + \varepsilon(e_\xi^T, s_\xi^T), \quad (24)$$

where

$$\tilde{W} = \hat{W} - W^*. \quad (25)$$

Theorem 2. Given the closed-loop dynamics defined by (24), the control input given in (23) and the adaptation law in (22) ensure an exponentially stable (ES) result of the tracking error e_{ξ} .

Proof of Theorem 2. Define the Lyapunov candidate function $V_{\xi} \in \mathbb{R}$ as

$$V_{\xi} = \frac{1}{2} s_{\xi}^T s_{\xi} + \frac{1}{2} \text{tr}(\tilde{W}^T \Gamma_{\xi}^{-1} \tilde{W}). \quad (26)$$

After taking the time derivative of (26) and substituting (24) together with (22) into the resulting equation, the following expression can be obtained:

$$\begin{aligned} \dot{V}_{\xi} &= s_{\xi}^T \dot{s}_{\xi} + \text{tr}(\tilde{W}^T \Gamma_{\xi}^{-1} \dot{\tilde{W}}) \\ &\leq -k_{\xi} \|s_{\xi}\|^2 + \frac{1}{2} \|s_{\xi}\|^2 + \frac{1}{2} \|\varepsilon(\cdot)\|^2 - \frac{\sigma_{\xi}}{2} \text{tr}(\tilde{W}^T \tilde{W}) + \frac{\sigma_{\xi}}{2} \text{tr}(W^{*T} W^*). \end{aligned} \quad (27)$$

Let $\Delta(t) = \frac{1}{2} \|s_{\xi}\|^2 + \frac{1}{2} \|\varepsilon(\cdot)\|^2 + \frac{\sigma_{\xi}}{2} \text{tr}(W^{*T} W^*)$; then the following inequality is obtained as

$$\|\Delta(t)\| \leq c, \quad (28)$$

where c is a positive constant. Then,

$$\begin{aligned} \dot{V}_{\xi} &\leq -k_{\xi} \|s_{\xi}\|^2 - \frac{\sigma_{\xi}}{2} \text{tr}(\tilde{W}^T \tilde{W}) + c \\ &\leq -a V_{\xi} + c, \end{aligned} \quad (29)$$

where

$$a = \min\{2k_{\xi}, \sigma_{\xi} \Gamma_{\xi}\}. \quad (30)$$

After solving the inequality (29), the following inequality is obtained:

$$V_{\xi}(t) \leq e^{-at} V(0) + \frac{c}{a} (1 - e^{-at}). \quad (31)$$

From the above inequality, it can be proven that (i) these errors $s_{\xi}(t)$, $\tilde{W}(t)$ are semiglobally uniformly ultimately bounded (SGUUB); (ii) the filtered error $s_{\xi}(t)$ is exponentially stable when choosing large enough design parameters; (iii) according to (12), the tracking error e_{ξ} is also exponentially stable, which is stronger than asymptotical stability. \square

After the above analysis, for the outer-loop position control, the RBFNN is utilized to estimate the actuator anomalies and external disturbances, and then the state feedback controller is employed for the position tracking control of the UAV.

3.2. Inner-Loop Attitude Controller Design Based on RISE Method

For the system $\dot{s}_{\eta} = f_{\eta}(\dot{e}_{\eta}, \tilde{\tau}, \dot{\eta}_d)$, the objective is to design the control scheme $\tilde{\tau}$ to ensure the asymptotic convergence of the tracking error e_{η} in (18). Before presenting the control law, some auxiliary error signals are defined first. The new filtered signal is denoted by $r_{\eta}(t) = [r_{\phi}(t) \quad r_{\theta}(t) \quad r_{\psi}(t)]^T \in \mathbb{R}^3$ is calculated as

$$r_{\eta} = s_{\eta} + \beta_{\eta} e_{\eta}. \quad (32)$$

Take the roll channel as an example in the following analysis. It can be concluded that

$$s_{\phi} = \dot{e}_{\phi} + \alpha_{\phi} e_{\phi}, \quad (33)$$

$$r_{\phi} = \dot{s}_{\phi} + \beta_{\phi} s_{\phi}, \quad (34)$$

After taking the time derivative of $r_{\phi}(t)$ and substituting (33) into the resulting equation, the following equation is obtained:

$$\dot{r}_{\phi} = \dot{\tilde{\tau}}_{\phi} + \dot{D}_{\phi} - \ddot{\phi}_d + \alpha_{\phi} \ddot{e}_{\phi} + \beta_{\phi} \dot{s}_{\phi}. \quad (35)$$

Let the auxiliary functions denoted by $N_\phi(\phi^{(i)}, t) \in \mathbb{R}$, $N_{d\phi}(t) \in \mathbb{R}$ and $\tilde{N}_\phi(t) \in \mathbb{R}$ be defined as follows:

$$N_\phi(\phi^{(i)}, t) = -\ddot{\phi}_d + \dot{D}_\phi + \alpha_\phi \ddot{e}_\phi + \beta_\phi \dot{s}_\phi + s_\phi, \quad (36)$$

$$N_{d\phi}(t) = -\ddot{\phi}_d + \dot{D}_\phi, \quad (37)$$

$$\tilde{N}_\phi(t) = N_\phi - N_{d\phi} = \alpha_\phi \ddot{e}_\phi + \beta_\phi \dot{s}_\phi + s_\phi. \quad (38)$$

Substituting (36)–(38) into (35), the open-loop error dynamics of the roll channel are obtained as

$$\dot{r}_\phi = -s_\phi + \dot{\tau}_\phi + N_{d\phi} + \tilde{N}_\phi. \quad (39)$$

Based on (39), the controller $\tilde{\tau}_\phi(t)$ is designed as

$$\tilde{\tau}_\phi = -(g_\phi + 1)(s_\phi(t) - s_\phi(0)) - \int_0^t [(g_\phi + 1)(\beta_\phi s_\phi(\tau) + h_\phi \text{sign}(s_\phi(\tau)))] d\tau. \quad (40)$$

where $g_\phi \in \mathbb{R}$ and $h_\phi \in \mathbb{R}$ are some positive gains.

Substituting (40) into (39), the closed-loop error dynamics of the roll channel are obtained as

$$\dot{r}_\phi = -s_\phi - (g_\phi + 1)r_\phi - h_\phi \text{sign}(s_\phi) + N_{d\phi} + \tilde{N}_\phi. \quad (41)$$

Remark 2. Since $\tilde{N}_\phi(s_\phi, r_\phi)$ is continuously differentiable, it satisfies the following inequality [32]:

$$\|\tilde{N}_\phi(s_\phi, r_\phi)\| \leq \rho_\phi(\varkappa_\phi) \|\varkappa_\phi\|, \quad (42)$$

where

$$\varkappa_\phi = [s_\phi \quad r_\phi]^T, \quad (43)$$

and the function $\rho_\phi(\cdot) : \mathbb{R}^+ \rightarrow \mathbb{R}^+$ is an invertible non-decreasing function.

Theorem 3. Considering the system (39), if the control gains h_ϕ is selected to satisfy the following condition:

$$h_\phi > \|N_{d\phi}\|_\infty + \frac{1}{\beta_\phi} \|\dot{N}_{d\phi}\|_\infty, \quad (44)$$

then the control laws in (40) ensure the closed-loop system (41) is semi-globally asymptotically stable.

Proof of Theorem 3. Let the auxiliary function $A_{u\phi}(t) \in \mathbb{R}$ be defined as

$$A_{u\phi} = A_{0\phi} - \int_0^t r_\phi(\tau)(N_{d\phi}(\tau) - h_\phi \text{sign}(s_\phi(\tau))) d\tau, \quad (45)$$

where

$$A_{0\phi} = h_\phi |s_\phi(0)| - s_\phi(0) N_{d\phi}(0). \quad (46)$$

Based on the analysis in [32], it is not difficult to check that $A_{u\phi}(t) \geq 0$. Let the Lyapunov function candidate denoted by $V_\phi(\zeta_\phi, t) \in \mathbb{R}$ be defined as

$$V_\phi(\zeta_\phi, t) = \frac{1}{2} s_\phi^2 + \frac{1}{2} r_\phi^2 + A_{u\phi}, \quad (47)$$

where

$$\zeta_\phi = \left[\varkappa_\phi^T \quad \sqrt{A_{u\phi}} \right]^T. \quad (48)$$

It is not difficult to obtain that $V_\phi(\zeta_\phi, t)$ is bounded by the following inequalities:

$$\frac{1}{2} \|\zeta_\phi\|^2 \leq V_\phi \leq \|\zeta_\phi\|^2. \quad (49)$$

After taking the time derivative of (47) and substituting (33), (41) together with (45) into the resulting equation, the following inequality can be obtained:

$$\begin{aligned}\dot{V}_\phi &= s_\phi \dot{s}_\phi + r_\phi \dot{r}_\phi + \dot{A}_{u\phi} \\ &\leq -k_{f\phi} \|\varkappa_\phi\|^2,\end{aligned}\quad (50)$$

where

$$k_{m\phi} = \min\{\beta_\phi, 1\}, \quad k_{f\phi} = k_{m\phi} - \frac{\rho_\phi^2(\varkappa_\phi)}{4g_\phi}.\quad (51)$$

If the control gain $k_{m\phi}$ satisfies the following inequality:

$$k_{m\phi} > \frac{\rho_\phi^2(\varkappa_\phi)}{4g_\phi},\quad (52)$$

it can be concluded that $k_{f\phi}(t) > 0$ and $\dot{V}_\phi(t) \leq 0$. Following Lemma 2 in [32], let the auxiliary functions $W_{1\phi}(\zeta_\phi)$, $W_{2\phi}(\zeta_\phi)$, and $W_\phi(\zeta_\phi)$ be defined as

$$\begin{cases} W_{1\phi}(\zeta_\phi) = \frac{1}{2} \|\zeta_\phi\|^2 \\ W_{2\phi}(\zeta_\phi) = \|\zeta_\phi\|^2 \\ W_\phi(\zeta_\phi) = -k_{f\phi} \|\varkappa_\phi\|^2 \end{cases},\quad (53)$$

and the region R_ϕ be defined as

$$R_\phi = \{\zeta_\phi \in \mathbb{R}^3 \mid \|\zeta_\phi\| < \rho_\phi^{-1}(2\sqrt{g_\phi k_{m\phi}})\}.\quad (54)$$

From (47) and (50), it can be concluded that $V_\phi(\zeta_\phi) \in \mathcal{L}_\infty$; thus $s_\phi(t) \in \mathcal{L}_\infty$ and $r_\phi(t) \in \mathcal{L}_\infty$. Then, from (33), it is not difficult to know that $\dot{s}_\phi(t) \in \mathcal{L}_\infty$ and $\dot{r}_\phi(t) \in \mathcal{L}_\infty$. Furthermore, the boundedness of $\dot{u}_\phi(t) \in \mathcal{L}_\infty$ and $\dot{r}_\phi(t) \in \mathcal{L}_\infty$ can be concluded from (35) and (40). From the definition of $W_\phi(\zeta_\phi)$, it can be concluded that $\dot{W}_\phi(\zeta_\phi) \in \mathcal{L}_\infty$, so $W_\phi(\zeta_\phi)$ is uniformly continuous. Let the convergence region denoted by S_ϕ be defined as

$$S_\phi : \{\zeta_\phi \in R_\phi, W_2(\zeta_\phi) < \frac{1}{2}(\rho_\phi^{-1}(2\sqrt{g_\phi k_{m\phi}}))^2\}.\quad (55)$$

Therefore, it can be concluded that

$$\lim_{t \rightarrow \infty} \varkappa_\phi(t) = 0.\quad (56)$$

Then from (43), it can be obtained that

$$\lim_{t \rightarrow \infty} s_\phi(t) = 0, \quad \lim_{t \rightarrow \infty} r_\phi(t) = 0.\quad (57)$$

Finally, from the linear filters in (33), it can be concluded that

$$\lim_{t \rightarrow \infty} e_\phi(t) = 0.\quad (58)$$

In the same way, the control inputs of pitch and yaw channel represented by $\tilde{\tau}_\theta(t)$ and $\tilde{\tau}_\psi(t)$ are designed as

$$\tilde{\tau}_\theta = -(g_\theta + 1)(s_\theta(t) - s_\theta(0)) - \int_0^t [(g_\theta + 1)(\beta_\theta s_\theta(\tau) + h_\theta \text{sign}(s_\theta(\tau)))] d\tau.\quad (59)$$

$$\tilde{\tau}_\psi = -(g_\psi + 1)(s_\psi(t) - s_\psi(0)) - \int_0^t [(g_\psi + 1)(\beta_\psi s_\psi(\tau) + h_\psi \text{sign}(s_\psi(\tau)))] d\tau.\quad (60)$$

where $g_\phi \in \mathbb{R}$, $h_\phi \in \mathbb{R}$, $g_\psi \in \mathbb{R}$, and $h_\psi \in \mathbb{R}$ are some positive gains.

$$\lim_{t \rightarrow \infty} e_\theta(t) = 0, \quad \lim_{t \rightarrow \infty} e_\psi(t) = 0.\quad (61)$$

□

In this section, the robust control method based on RISE is designed for the inner-loop attitude control to compensate for actuator anomalies and external disturbances.

4. Stability Analysis

Due to the existence of the coupling term $\Delta(F, \eta_d, e_\eta)$, Theorems 1 and 2 cannot be used to determine the stability of the closed-loop system directly. Hence, the following lemma is invoked to analyze the stability of the cascaded systems.

Lemma 1. *If there is a feedback v such that $s_{\bar{\zeta}} = 0$ is an asymptotically stable equilibrium of $\dot{s}_{\bar{\zeta}} = f_{\bar{\zeta}}(\bar{e}_{\bar{\zeta}}, v, \bar{\zeta}_d)$, then any partial-state feedback control $\tilde{\tau}$ that renders the s_η -subsystem equilibrium $s_\eta = 0$ asymptotically stable also achieves asymptotic stability of $(s_{\bar{\zeta}}(t), s_\eta(t)) = (0, 0)$.*

Proof of Lemma 1. See the proof in [33]. \square

Therefore, the stability of the connected system (16) and (20) will be ensured if we prove that all the trajectories $(s_{\bar{\zeta}}(t), s_\eta(t))$ are bounded. Then, the following lemma will be introduced.

Lemma 2. *Let $\tilde{\tau}$ be any L^1 partial-state feedback such that the equilibrium point $s_\eta = 0$ is globally asymptotically stable (GAS). Suppose that there exist a constant $c_1 \in R^+$ and a class- κ function $\kappa(\cdot)$ that is differentiable at $s_\eta = 0$ such that*

$$\|s_{\bar{\zeta}}\| \geq c_1 \Rightarrow \|\Delta(s_{\bar{\zeta}}, r_\eta)\| \leq \kappa(\|r_\eta\|)\|s_{\bar{\zeta}}\|. \tag{62}$$

If there exists a positive semi-definite radially unbounded function $V_s(s_{\bar{\zeta}})$ and $c_2, c_3 \in R^+$ such that for $\|s_{\bar{\zeta}}\| \geq c_2$,

$$\frac{\partial V_s}{\partial s_{\bar{\zeta}}} \cdot \dot{s}_{\bar{\zeta}} \leq 0, \tag{63}$$

$$\left\| \frac{\partial V_s}{\partial s_{\bar{\zeta}}} \right\| \cdot \|s_{\bar{\zeta}}\| \leq c_3 V_s(s_{\bar{\zeta}}). \tag{64}$$

the feedback $\tilde{\tau}$ guarantees the boundedness of all the solutions of (16) and (20).

Proof of Lemma 2. See the proof in [34]. \square

Therefore, the problem is reduced to ensuring that the closed-loop system controlled by v and $\tilde{\tau}$ satisfies (62)–(64) in the lemmas above.

From Theorem 1, the $s_{\bar{\zeta}}$ -subsystem without the interconnection term is globally exponentially stable (GES), which is stronger than the GAS property. The GES of the subsystem implies that there exist a positive definite radially unbounded function $V_s(s_{\bar{\zeta}})$ and positive constants c_2 and c_3 such that for $\|s_{\bar{\zeta}}\| \geq c_2 : \frac{\partial V_s}{\partial s_{\bar{\zeta}}} \cdot \dot{s}_{\bar{\zeta}} \leq 0$ and $\left\| \frac{\partial V_s}{\partial s_{\bar{\zeta}}} \right\| \cdot \|s_{\bar{\zeta}}\| \leq c_3 V_s(s_{\bar{\zeta}})$. Therefore, Conditions (63)–(64) of Theorem 2 are satisfied.

Now, it remains to be shown that the interconnection term $\Delta(s_{\bar{\zeta}}, r_\eta)$ satisfies the growth restriction of Lemma 2.

$$\begin{aligned} \|\Delta(s_{\bar{\zeta}}, r_\eta)\| &\leq \frac{1}{m} |F| \|h(\eta_d, e_\eta)\| \\ &= \frac{1}{m} |F| \sqrt{h_x^2 + h_y^2 + h_z^2}, \end{aligned} \tag{65}$$

where h_x, h_y, h_z are defined in (17), and then the following can be obtained as

$$|F| = m \sqrt{v_x^2 + v_y^2 + (v_z + g)^2}. \tag{66}$$

To prove the boundedness of the interconnection term $\Delta(s_{\bar{\zeta}}, r_\eta)$, the following two Lemmas are introduced.

Lemma 3. Since the desired trajectories $\xi_d(t)$ and their time-derivatives are bounded, there exist some positive constants c_4 and k_1 such that F satisfies the following properties:

$$|F| \leq \begin{cases} k_1 \|s_{\xi}\|, & \text{for } \|s_{\xi}\| \geq c_4 \\ k_1 c_4, & \text{for } \|s_{\xi}\| < c_4 \end{cases}. \quad (67)$$

Lemma 4. There exists a positive constant k_H such that the interconnection term $h(\eta_d, e_\eta)$ satisfies the following inequality:

$$\|h(\eta_d, e_\eta)\| \leq k_H \|e_\eta\|. \quad (68)$$

Proof of Lemmas 3 and 4. The proofs of Lemmas 3 and 4 can be found in [31,34]. \square

From Lemmas 3 and 4, we can write that for $\|s_{\xi}\| \geq c_4$, we have

$$\|F \cdot h(\eta_d, e_\eta)\| \leq k_1 \|s_{\xi}\| \cdot k_H \|e_\eta\| \leq k \|s_{\xi}\| \|e_\eta\|, \quad (69)$$

where $k = k_1 k_H$ is a positive constant. Finally, we obtain the following inequality

$$\begin{aligned} \|\Delta(s_{\xi}, r_\eta)\| &= \frac{1}{m} \|F \cdot h(\eta_d, e_\eta)\| \\ &\leq \gamma(\|e_\eta\|) \|s_{\xi}\|, \text{ for } \|s_{\xi}\| \geq c_4, \end{aligned} \quad (70)$$

where $\gamma(\|e_\eta\|) = \frac{k}{m} \|e_\eta\|$ is a class- κ function. Therefore, all the conditions of Lemma 1 are satisfied, and the asymptotic stability of $(s_{\xi}(t), s_\eta(t)) = (0, 0)$ is guaranteed.

After the above analysis, the composite stability of the cascaded system and the asymptotical tracking performance are proved via the Lyapunov-based stability analysis method.

5. Numerical Simulations

5.1. Simulation Results of the Proposed FTC Scheme

In this section, numerical simulations are implemented in Matlab to validate the performance of the proposed fault-tolerant tracking control design. The parameters of the tri-rotor UAV and the designed FTC strategy were listed as follows: $m = 0.5 \text{ kg}$, $J = \text{diag}\{[2.0 \ 8.3 \ 8.2]^T\} \times 10^{-3} \text{ kg} \cdot \text{m}^3$, $\alpha_\eta = [16 \ 16 \ 16]^T$, $\beta_\eta = [2 \ 2 \ 2]^T$, $g_\eta = [8 \ 8 \ 8]^T$, $h_\eta = [3 \ 3 \ 3]^T$, $\alpha_\xi = \text{diag}\{[3 \ 3 \ 3]^T\}$, $k_\xi = \text{diag}\{[20 \ 20 \ 20]^T\}$, $\sigma_\xi = 2.7$, $\Gamma_\xi = [0.2 \ 0.2 \ 0.2 \ 0.2 \ 0.2 \ 0.2 \ 0.2 \ 0.2 \ 0.2 \ 0.2]^T$.

The external disturbances were set as

$$D_\xi(t) = \begin{cases} [0 \ 0 \ 0]^T, & t \leq 10\text{s} \\ [0.4 \sin(t) \ 0.5 \cos(0.6t) \ 0.3 \cos(0.4t)]^T, & t > 10\text{s} \end{cases}, \quad (71)$$

$$D_\eta(t) = \begin{cases} [0 \ 0 \ 0]^T, & t \leq 10\text{s} \\ [0.2 \sin(0.5t) \ 0.4 \cos(0.6t) \ 0.3 \cos(t)]^T, & t > 10\text{s} \end{cases}. \quad (72)$$

The desired tracking targets are selected as

$$\xi_d(t) = [0.2 \cos(0.6t) \ 0.1 \cos(0.8t) \ 0.15 \cos(0.4t)]^T m \text{ and } \psi_d(t) = 0.5 \cos(0.7t) \text{ deg.}$$

During the simulation, the actuator anomalies of the tri-rotor UAV were introduced at the time of 15s, which was defined as follows:

$$\Lambda_\xi(t) = [0.3 \cos(0.5t) \ 0.2 \sin(0.6t) \ 0.4 \sin(0.5t)]^T,$$

$$\Lambda_\eta(t) = \text{diag}\{[0.3 \cos(0.6t) \ 0.5 \sin(0.7t) \ 0.3 \sin(0.7t)]^T\}, \text{ shown as Figures 2 and 3.}$$

The simulation results of the proposed FTC scheme are shown in Figures 4–7.

Figures 4 and 5 show the UAV's position and attitude tracking control performances. In Figure 4, it is shown that the current position can well follow the predefined trajectory even should actuator anomalies happen. In Figure 5, the current attitude can follow the desired attitude from the initial state quickly, and the tracking errors suddenly changes

within 1° when the actuator anomalies happen, which recovers to perfect tracking performance in about 4s. The robustness of the proposed FTC scheme can be tested and verified through inserting external disturbances of different amplitudes, which ensures the range of the variation and the response time within some reasonable values.

The control inputs, including the total thrust and torques, are illustrated in Figure 6. When the actuator anomalies happen, the thrust and torques produced by each motor change violently and then restore to their normal values. From Figure 7, the boundedness of RBFNN weights can be seen, which are coincident with (22).

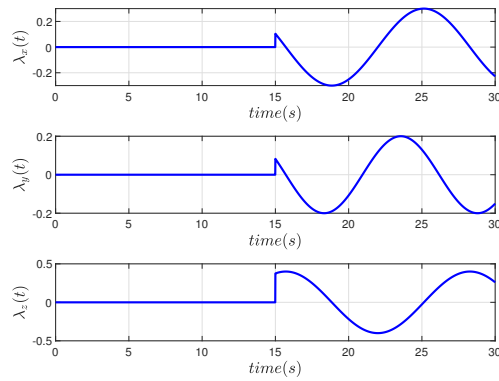


Figure 2. Actuator Anomalies for Position Channel.

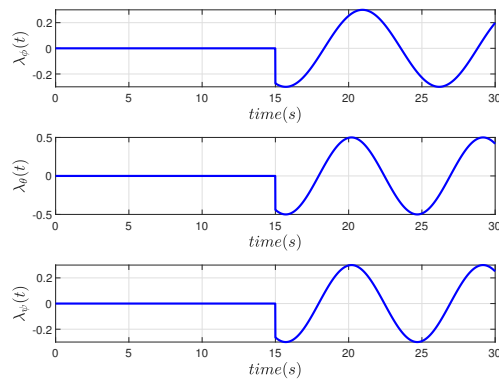


Figure 3. Actuator Anomalies for Attitude Channel.

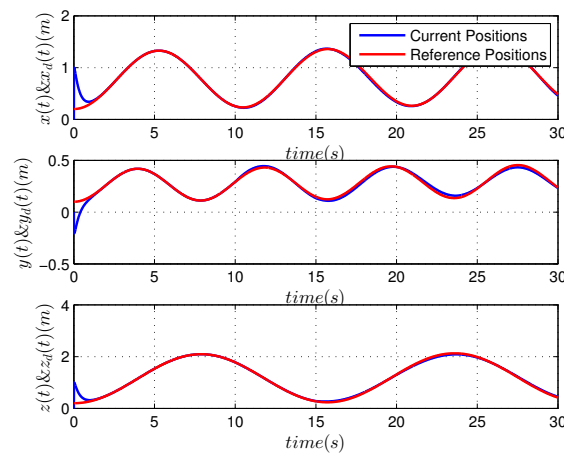


Figure 4. UAV's Position Tracking Performance.

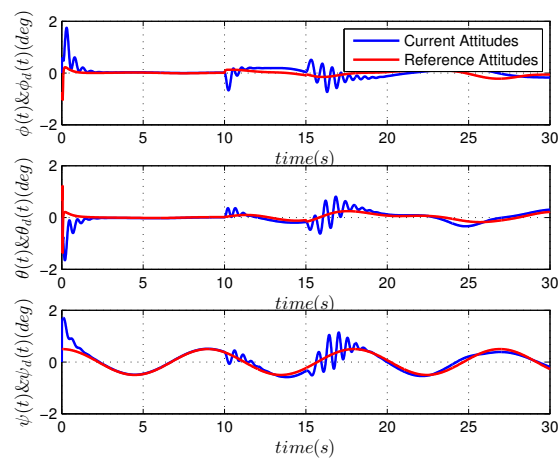


Figure 5. UAV's Attitude Tracking Performance.

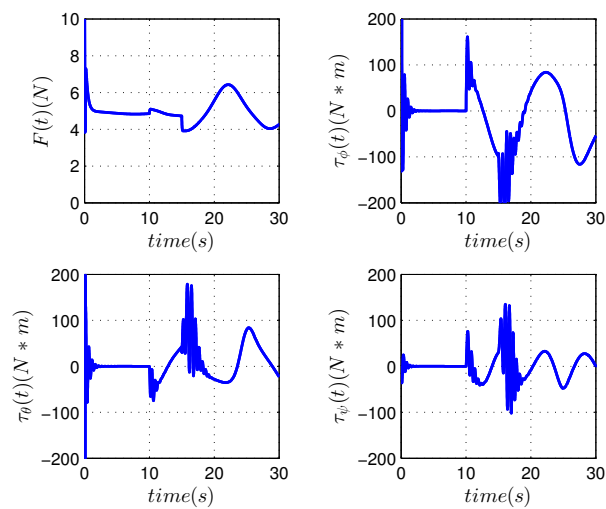


Figure 6. UAV's Control Inputs.

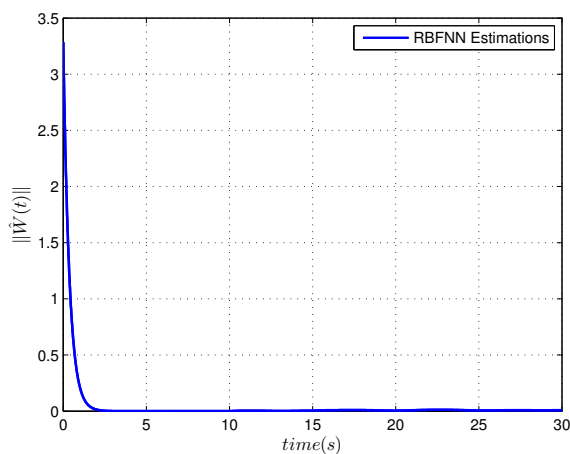


Figure 7. RBFNN Weights of Position Control.

5.2. Comparison and Analysis of the Results

For comparison purposes, an SM-based FTC scheme was implemented under identical circumstances. The simulation results are shown in Figures 8 and 9.

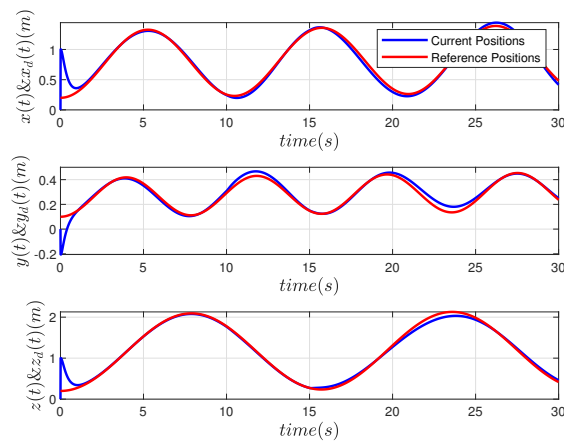


Figure 8. UAV's Position Tracking Performance: SM.

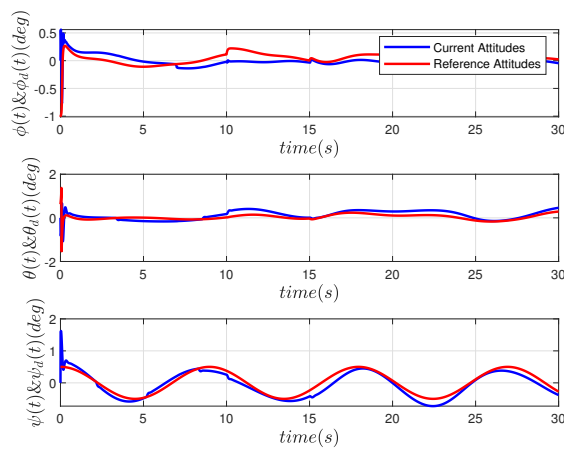


Figure 9. UAV's Attitude Tracking Performance: SM.

In order to quantitatively show the differences between the two controllers, the MAX offset and the root-mean-square (RMS) errors after the actuator anomalies happened were introduced and are listed in Table 1.

Table 1. Analysis of Control Errors.

Controller	RBFNN&RISE Based FTC Scheme	SM-Based FTC Scheme
<i>x</i> -axis MAX offset	0.03 m	0.05 m
<i>y</i> -axis MAX offset	0.02 m	0.12 m
<i>z</i> -axis MAX offset	0.05 m	0.08 m
Roll MAX offset	0.5°	0.3°
Pitch MAX offset	0.4°	0.5°
Yaw MAX offset	0.8°	0.5°
<i>x</i> -axis RMS error	0.0183	0.0420
<i>y</i> -axis RMS error	0.0168	0.0239
<i>z</i> -axis RMS error	0.0296	0.0600
Roll RMS error	0.1319	0.1872
Pitch RMS error	0.1430	0.1680
Yaw RMS error	0.1567	0.1784

From Table 1, it can be seen that most MAX offsets and RMS errors of the proposed control scheme are smaller than that of the SM controller. Thus, the effectiveness and better performance of the proposed FTC strategy are verified.

6. Conclusions

With the development of the tri-rotor UAV, actuator anomalies have become increasingly frequent. To solve this problem, the authors of the present study aimed to propose a robust trajectory tracking control method to realize the robust tracking control of the tri-rotor UAV under abnormal actuator behavior together with external disturbances, as few existing works have taken this into consideration. The actuator anomalies were modeled as time-varying multiplicative parameters to further improve modeling accuracy. RBFNN was utilized to compensate for the actuator anomalies and external disturbances, and then the feedback linearization method was employed for the outer-loop position tracking control. The RISE-based controller was then designed to realize the inner-loop attitude tracking control with actuator anomalies and external disturbances. A Lyapunov-based analysis was used to prove the composite stability of the cascaded system. Numerical simulations and a comparison with the SM control method validated the superior performance and robustness of the proposed control strategy. Future work will focus on other kinds of neural networks to estimate the unknown actuator anomalies and external disturbances and other nonlinear FTC designs. Furthermore, building the UAV testbed and real-time experimental verifications are also under consideration.

Author Contributions: Conceptualization, W.M. and W.H.; methodology, W.H. and H.W.; software, P.W.; validation, M.H., W.M. and W.H.; formal analysis, M.H.; investigation, P.W.; resources, H.W.; data curation, H.W. and W.H.; writing—original draft preparation, W.M.; writing—review and editing, W.H.; visualization, H.W.; supervision, M.H.; project administration, W.M.; funding acquisition, W.H. All authors have read and agreed to the published version of the manuscript.

Funding: This research was funded by the National Natural Science Foundation of China under grant number 62103060, the Natural Science Foundation of Shandong Province under Grant numbers ZR2019PF021 and ZR2020MF142 and China University Innovation Fund under grant number 2021ZYA07001.

Institutional Review Board Statement: Not applicable.

Informed Consent Statement: Not applicable.

Data Availability Statement: Not applicable.

Conflicts of Interest: The authors declare no conflict of interest.

References

1. Chen, F.; Jiang, R.; Zhang, K.; Jiang, B.; Tao, G. Robust backstepping sliding mode control and observer-based fault estimation for a quadrotor UAV. *IEEE Trans. Ind. Electron.* **2016**, *63*, 5044–5056. [\[CrossRef\]](#)
2. Liu, H.; Xi, J.; Zhong, Y. Robust attitude stabilization for nonlinear quadrotor systems with uncertainties and delays. *IEEE Trans. Ind. Electron.* **2017**, *64*, 5585–5594. [\[CrossRef\]](#)
3. Yoo, D.; Oh, H.; Won, D.; Tahk, M. Dynamic modeling and stabilization techniques for tri-rotor unmanned aerial vehicles. *Int. J. Aeronaut. Space Sci.* **2010**, *11*, 167–174. [\[CrossRef\]](#)
4. Gu, X.; Xian, B.; Li, J. Model free adaptive control design for a tilt trirotor unmanned aerial vehicle with quaternion feedback: Theory and implementation. *Int. J. Adapt. Control* **2022**, *36*, 122–137. [\[CrossRef\]](#)
5. Hao, W.; Ma, W.; Yuan, W.; Wang, H.; Du, Y. Modeling and nonlinear robust tracking control of a three-rotor UAV based on RISE method. *IEEE Access* **2021**, *9*, 38802–38809. [\[CrossRef\]](#)
6. Liu, Z.; He, Y.; Yang, L.; Han, J. Control techniques of tilt rotor unmanned aerial vehicle systems: A review. *Chin. J. Aeronaut.* **2017**, *30*, 135–148. [\[CrossRef\]](#)
7. Yu, L.; He, G.; Zhao, S.; Wang, X. Dynamic inversion-based sliding mode control of a tilt tri-rotor UAV. In Proceedings of the Asian Control Conference (ASCC), Kitakyushu, Japan, 9–12 June 2019; p. 18849170.
8. Sun, N.; Yang, T.; Fang, Y.; Wu, Y.; Chen, H. Transportation control of double-pendulum cranes with a nonlinear quasi-PID scheme: Design and experiments. *IEEE Trans. Syst. Man Cybern. Syst.* **2019**, *49*, 1408–1418. [\[CrossRef\]](#)
9. Xian, B.; Yang, S. Robust tracking control of a quadrotor unmanned aerial vehicle-suspended payload system. *IEEE/ASME Trans. Mech.* **2021**, *26*, 2653–2663. [\[CrossRef\]](#)
10. Salazar-Cruz, S.; Kendoul, F.; Lozano, R.; Fantoni, I. Real-time stabilization of a small three-rotor aircraft. *IEEE Trans. Aerosp. Electron. Syst.* **2008**, *44*, 783–794. [\[CrossRef\]](#)

11. Papachristos, C.; Alexis, K.; Tzes, A. Linear quadratic optimal position control for an unmanned tri-TiltRotor. In Proceedings of the International Conference Control, Decision and Information Technologies (CoDIT), Hammamet, Tunisia, 6–8 May 2013; pp. 708–713.
12. Ali, Z.; Wang, D.; Masroor, S.; Loya, M. Attitude and altitude control of trirotor UAV by using adaptive hybrid controller. *J. Control Sci. Eng.* **2016**, *2016*, 6459891.1–12. [[CrossRef](#)]
13. Yu, B.; Zhang, Y.; Qu, Y. Fault tolerant control using PID structured optimal technique against actuator faults in a quadrotor UAV. In Proceedings of the International Conference on Unmanned Aircraft Systems (ICUAS), Orlando, FL, USA, 27–30 May 2014; pp. 167–174.
14. He, A.; Zhang, Y.; Zhao, H.; Wang, B.; Gao, Z. Adaptive fault-tolerant control of a hybrid VTOL UAV against actuator faults and model uncertainties under fixed-wing mode. *Int. J. Aerospace Eng.* **2022**, *10*, 8191154. [[CrossRef](#)]
15. Zou, Y. Nonlinear robust adaptive hierarchical sliding mode control approach for quadrotors. *Int. J. Robust Nonlin.* **2016**, *27*, 925–941. [[CrossRef](#)]
16. Guo, J.; Qi, J.; Wu, C. Robust fault diagnosis and fault-tolerant control for nonlinear quadrotor unmanned aerial vehicle system with unknown actuator faults. *Int. J. Adv. Robot. Syst.* **2021**, *2*, 1–14. [[CrossRef](#)]
17. Zhang, Y.; Chamseddine, A.; Rabbath, C. Development of advanced FDD and FTC techniques with application to an unmanned quadrotor helicopter testbed. *J. Frank. Inst.* **2013**, *350*, 2396–2422. [[CrossRef](#)]
18. Yu, Z.; Zhang, Y.; Jiang, B.; Fu, J.; Jin, Y. A review on fault-tolerant cooperative control of multiple unmanned aerial vehicles. *Chin. J. Aeronaut.* **2021**, *35*, 1–18. [[CrossRef](#)]
19. Zhao, W.; Liu, H.; Lewis, F. Data-driven fault-tolerant control for attitude synchronization of nonlinear quadrotors. *IEEE Trans. Autom. Control.* **2021**, *66*, 5584–5591. [[CrossRef](#)]
20. Nguyen, T.; Saussie, D.; Saydy, L. Design and experimental validation of robust self-scheduled fault-tolerant control laws for a multicopter UAV. *IEEE/ASME Trans. Mech.* **2021**, *26*, 2548–2557. [[CrossRef](#)]
21. Zou, Y.; Xia, R. Robust fault-tolerant control for underactuated takeoff and landing UAVs. *IEEE Trans. Aero. Elec. Sys.* **2020**, *56*, 3545–3555. [[CrossRef](#)]
22. Shen, Q.; Jiang, B.; Shi, P. Active fault-tolerant control against actuator fault and performance analysis of the effect of time delay due to fault diagnosis. *Int. J. Contr. Autom.* **2017**, *15*, 537–546. [[CrossRef](#)]
23. Falcon, G.; Holzapfel, F. Adaptive fault tolerant control allocation for a hexacopter system. In Proceedings of the 2016 American Control Conference (ACC), Boston, MA, USA, 6–8 July 2016; pp. 6760–6766.
24. Xian, B.; Hao, W. Nonlinear robust fault-tolerant control of the tilt trirotor UAV under rear servo's stuck fault: Theory and experiments. *IEEE Trans. Ind. Informat.* **2019**, *15*, 2158–2166. [[CrossRef](#)]
25. Hao, W.; Xian, B.; Xie, T. Fault tolerant position tracking control design for a tilt tri-rotor unmanned aerial vehicle. *IEEE Trans. Ind. Electron.* **2022**, *69*, 604–612. [[CrossRef](#)]
26. Xian, B.; Diao, C.; Zhao, B.; Zhang, Y. Nonlinear robust output feedback tracking control of a quadrotor UAV using quaternion representation. *Nonlinear Dynam.* **2015**, *79*, 2735–2752. [[CrossRef](#)]
27. Wen, G.; Hao, W.; Feng, W.; Gao, K. Optimized backstepping tracking control using reinforcement learning for quadrotor unmanned aerial vehicle system. *IEEE Trans. Syst. Man Cy.-S.* **2022**, *52*, 5004–5015. [[CrossRef](#)]
28. Cai, Z.; de Queiroz, M.; Dawson, D. A sufficiently smooth projection operator. *IEEE Trans. Autom. Control* **2006**, *51*, 135–139. [[CrossRef](#)]
29. Kendoul, F.; Yu, Z.; Nonami, K. Guidance and nonlinear control system for autonomous flight of minirotorcraft unmanned aerial vehicles. *J. Field Robot.* **2010**, *27*, 311–334. [[CrossRef](#)]
30. Sontag, E. Smooth stabilization implies coprime factorization. *IEEE Trans. Autom. Control* **1988**, *34*, 435–443. [[CrossRef](#)]
31. Zhao, B.; Xian, B.; Zhang, Y.; Zhang, X. Nonlinear robust adaptive tracking control of a quadrotor UAV via immersion and invariance methodology. *IEEE Trans. Ind. Electron.* **2015**, *62*, 2891–2902. [[CrossRef](#)]
32. Xian, B.; Dawson, D.; de Queiroz, M.; Chen, J. Continuous asymptotic tracking control strategy for uncertain multi-input nonlinear systems. *IEEE Trans. Autom. Control* **2004**, *49*, 1206–1211. [[CrossRef](#)]
33. Sepulchre, R.; Jankovic, M.; Kokotovic, P. *Constructive Nonlinear Control*; Springer: New York, NY, USA, 1997.
34. Kendoul, F. Nonlinear hierarchical flight controller for unmanned rotorcraft: Design, stability, experiments. *J. Guid. Control Dynam.* **2009**, *32*, 1954–1958. [[CrossRef](#)]

Disclaimer/Publisher's Note: The statements, opinions and data contained in all publications are solely those of the individual author(s) and contributor(s) and not of MDPI and/or the editor(s). MDPI and/or the editor(s) disclaim responsibility for any injury to people or property resulting from any ideas, methods, instructions or products referred to in the content.